Free Radical Biology and Medicine 72 (2014) 55–65

Contents lists available at ScienceDirect

Free Radical Biology and Medicine

journal homepage: www.elsevier.com/locate/freeradbiomed

Original Contribution

Redox proteomic identification of HNE-bound mitochondrial proteins in cardiac tissues reveals a systemic effect on energy metabolism after doxorubicin treatment

Y. Zhao [a], S. Miriyala [a,b], L. Miao [a], M. Mitov [c], D. Schnell [a], S.K. Dhar [a], J. Cai [d], J.B. Klein [d], R. Sultana [e], D.A. Butterfield [c,e], M. Vore [a], I. Batinic-Haberle [f], S. Bondada [g], D.K. St. Clair [a,*]

[a] Graduate Center for Toxicology, University of Kentucky, Lexington, KY 40506, USA
[b] Department of Cellular Biology and Anatomy, Louisiana State University Health Sciences, Shreveport, LA 71130, USA
[c] Free Radical Biology in Cancer Shared Resource Facility, Markey Cancer Center, University of Kentucky, Lexington, KY 40506, USA
[d] Department of Nephrology and Proteomics Facility, University of Louisville, Louisville, KY 40292, USA
[e] Department of Chemistry, Center of Membrane Sciences, and Sanders-Brown Center on Aging, University of Kentucky, Lexington, KY 40506, USA
[f] Department of Radiation Oncology, Duke University School of Medicine, Durham, NC 27710, USA
[g] Department of Immunology, University of Kentucky, Lexington, KY 40506, USA

ARTICLE INFO

Article history:
Received 16 September 2013
Received in revised form
17 February 2014
Accepted 4 March 2014
Available online 12 March 2014

Keywords:
Doxorubicin
Cardiac injury
ATP synthase
Dihydrolipoyl dehydrogenase
Succinate dehydrogenase [ubiquinone] flavoprotein
NADH dehydrogenase [ubiquinone] iron–sulfur protein 2
Oxidative stress
Redox proteomics
Free radicals
Metabolism

ABSTRACT

Doxorubicin (DOX), one of the most effective anticancer drugs, is known to generate progressive cardiac damage, which is due, in part, to DOX-induced reactive oxygen species (ROS). The elevated ROS often induce oxidative protein modifications that result in alteration of protein functions. This study demonstrates that the level of proteins adducted by 4-hydroxy-2-nonenal (HNE), a lipid peroxidation product, is significantly increased in mouse heart mitochondria after DOX treatment. A redox proteomics method involving two-dimensional electrophoresis followed by mass spectrometry and investigation of protein databases identified several HNE-modified mitochondrial proteins, which were verified by HNE-specific immunoprecipitation in cardiac mitochondria from the DOX-treated mice. The majority of the identified proteins are related to mitochondrial energy metabolism. These include proteins in the citric acid cycle and electron transport chain. The enzymatic activities of the HNE-adducted proteins were significantly reduced in DOX-treated mice. Consistent with the decline in the function of the HNE-adducted proteins, the respiratory function of cardiac mitochondria as determined by oxygen consumption rate was also significantly reduced after DOX treatment. Treatment with Mn(III) *meso*-tetrakis(*N*-*n*-butoxyethylpyridinium-2-yl)porphyrin, an SOD mimic, averted the doxorubicin-induced mitochondrial dysfunctions as well as the HNE–protein adductions. Together, the results demonstrate that free radical-mediated alteration of energy metabolism is an important mechanism mediating DOX-induced cardiac injury, suggesting that metabolic intervention may represent a novel approach to preventing cardiac injury after chemotherapy.

Doxorubicin (DOX), one of the most effective anticancer drugs, has been a therapeutic for a broad spectrum of human cancers for almost half a century and remains the first choice for many aggressive tumors, such as acute myeloid leukemia [1]. Its clinical application is highly limited owing to the dose-related, progressive, and irreversible cardiac damage it causes. The mortality of patients who develop congestive heart failure after DOX treatments can be as high as 50% [2], increasing significantly when cumulative doses are more than 500 mg/m^2 [3].

Numerous studies have focused on the mechanisms behind DOX-induced cardiotoxic effects and demonstrated multifactorial causes. However, there is consensus that oxidative stress is a primary mechanism of DOX-induced cardiotoxicity and that the stress is attributed to the formation of reactive oxygen species (ROS). DOX generates ROS by various means, mainly through redox cycling. The quinone moiety of DOX can be converted one-electronically to semiquinone by several cellular oxidoreductases [4]. One-electron

Abbreviations: DOX, doxorubicin; ATP5B, ATP synthase subunit β; DLD, dihydrolipoyl dehydrogenase; SDHA, succinate dehydrogenase [ubiquinone] flavoprotein subunit; NDUFS2, NADH dehydrogenase [ubiquinone] iron–sulfur protein 2; ROS, reactive oxygen species; HNE, 4-hydroxy-2-nonenal; TCA cycle, citric acid cycle; ETC, electron transport chain; OCR, oxygen consumption rate; ECAR, extracellular acidification rate; FH, fumarate hydratase; HADHA, trifunctional enzyme subunit α; CKMT2, creatine kinase S-type; Oxct1, 3-oxoacid–CoA transferase 1; MnP, Mn(III) *meso*-tetrakis(*N*-*n*-butxyethylpyridinum-2-yl) porphyrin or MnTnBuOE-2-PyP^{5+}; NAC, *N*-acetylcysteine

* Corresponding author. Fax: +1 859 323 1059.
E-mail address: dstcl00@uky.edu (D.K. St. Clair).

http://dx.doi.org/10.1016/j.freeradbiomed.2014.03.001
0891-5849/

oxidation of the DOX-semiquinone radical to the DOX-quinone form leads to the generation of a highly reactive superoxide, which can be further involved in the production of a variety of ROS, including $OH^{\bullet}$, $ROO^{\bullet}$, $ONOO^{-}$, ROOH, and H_2O_2 [5].

ROS are highly reactive with biomolecules, including lipids, proteins, carbohydrates, DNA, and RNA, and lead to cellular dysfunction [6]. A major source of ROS-mediated injury is lipid peroxidation, the reaction of ROS with the polyunsaturated fatty acids of lipid membranes. Lipid peroxidation generates a number of cytotoxic and highly reactive by-products such as aldehydes, alkenals, and hydroxyalkenals. Among lipid peroxidation products, 4-hydroxy-2-nonenal (HNE) is the most abundant [7]. HNE readily reacts with proteins and, at higher concentrations, with DNA [8,9]. HNE has a high affinity for and covalently attaches to Cys, His, and Lys residues by the Michael addition [10], which leads to dysfunction in the target proteins linked to intracellular signal transduction, aging, and many human diseases.

Cardiomyocytes have more mitochondria, in both number and volume, than other cells, and they are the most active cells with regard to the oxidative phosphorylation that is required for their energy needs [11]. The complex that DOX forms with cardiolipin, which resides in the mitochondrial inner membrane [12], places DOX in close proximity to the mitochondrial electron transport chain. The redox cycling of DOX is mediated through its interaction with NADH dehydrogenase (complex I) of the mitochondrial electron transport chain (ETC) [13]. Thus, active mitochondria are both important sources and primary targets of DOX-induced ROS. Multiple studies indicate that mitochondrial dysfunction is a key factor in the process of DOX-induced pathogenicity [14–16]. Studies utilizing tissue samples from patients receiving DOX reveal histopathological evidence that suggests disruption of mitochondrial structure and membranes [17]; similar observations were made in animal models and in cells in vitro [8,18].

HNE–protein adductions play important roles in regulating the function of proteins that may lead to cellular dysfunction. In this study, we used two-dimensional (2D) electrophoresis and redox immunochemistry analysis followed by mass spectrometry and interrogation of protein databases to identify eight HNE-adducted proteins in mouse heart mitochondria after DOX treatment. We then verified the consequences of HNE adduction on the functions of those proteins via enzymatic activity assays as well as on mitochondrial function.

Materials and methods

Materials

Doxorubicin was obtained from Bedford Laboratories (Bedford, OH, USA). Succinate dehydrogenase [ubiquinone] flavoprotein subunit (SDHA), dihydrolipoyl dehydrogenase (DLD), and fumarate hydratase (FH) antibodies were purchased from Santa Cruz Biotechnology (Santa Cruz, CA, USA). MnTnBuOE-2-PyP^{5+} (MnP) was produced by Dr. Ines Batinic-Haberle of the Department of Radiation Oncology, Duke University. *N*-acetylcysteine (NAC) and ATP synthase antibody were purchased from Sigma (St. Louis, MO, USA). NADH dehydrogenase [ubiquinone] iron–sulfur protein 2 (NDUFS2) and HNE antibodies and complex I and ATP synthase activity assay kits were purchased from Abcam (Cambridge, MA, USA); H9C2, a neonatal rat heart cell line, was from the ATCC (Manassas, VA, USA).

Animal treatment and mitochondrial isolation

All animals were housed in the University of Kentucky Animal Facility and experiments were conducted using procedures approved by Institutional Animal Care in accordance with the NIH *Guide for the Care and Use of Laboratory Animals.* In-house bred, 9-week-old, male, C57BL/6 mice were treated with a single dose of 20 mg/kg DOX or saline via intraperitoneal injection. Seventy-two hours after injection, mice were euthanized.

Heart mitochondria were isolated as described previously [19]. Briefly, freshly isolated hearts were washed in ice-cold isolation buffer (0.225 M mannitol, 0.075 M sucrose, 1 mM EGTA, pH 7.4) and homogenized at 500 rpm with a chilled Teflon pestle for 10 strokes in isolation buffer. The homogenate was centrifuged at 480 *g* at 4 °C for 5 min in a Sorval SS 34 rotor. The resulting supernatant was filtered through double-layered cheesecloth and centrifuged at 7700 *g* at 4 °C for 10 min. The pellet was washed twice by gentle resuspension in 3 ml isolation buffer and centrifuged at 7700 *g* at 4 °C for 10 min. The resulting mitochondria were either used or frozen in liquid nitrogen for further analysis. The purity of mitochondria was examined using lamin A (nuclear protein) and IκB-α (cytoskeletal protein) on Western blot.

Total protein-bound HNE detection

The levels of total protein-bound HNE were determined in the Free Radical Biology in Cancer Shared Resource Facility (FRBC SRF) at the University of Kentucky. The mitochondrial samples (pellets) were thawed and resuspended in a small volume (75–150 μl) of ice-cold homogenization buffer (0.32 M sucrose, 10 mM Hepes, pH 7.4, 2 mM EDTA, protease inhibitors). Five microliters of the homogenized sample was mixed and diluted with an equal volume of 12% SDS. Samples were further denatured with 10 μl of modified Laemmli buffer (0.125 M Trizma base, 4% SDS, and 20% glycerol) for 20 min at room temperature. Next, 250 ng of the derivatized protein was loaded in each slot (48-well slot format Bio-Dot SF apparatus with nitrocellulose membranes, pore size 0.2 μm, Bio-Rad, Hercules, CA, USA). The antibody reaction was developed using 5-bromo-4-chloro-3-indolyl phosphate in conjunction with nitroblue tetrazolium. The immunodetection was performed by using 1:5000 anti-4-hydroxynonenal antiserum (Alpha Diagnostic International, San Antonio, TX, USA) and goat 1:7500 anti-rabbit IgG (Sigma–Aldrich) antibody for the secondary detection. The nitrocellulose membranes were scanned by photo scanner (Epson Perfection V600, Long Beach, CA, USA), and slot-blot line densities were quantified by the ImageQuant TL software package (GE Healthcare Bio-Sciences, Piscataway, NJ, USA).

Two-dimensional gel electrophoresis and protein mass spectrometry studies

Two-dimensional gel electrophoresis was performed in the core facility of FRBC SRF using a protocol similar to that previously described [20]. Briefly, a duplicate amount (150 μg protein) of each isolated mitochondrial sample underwent trichloroacetic acid precipitation and rehydration in 2D gel rehydration medium (8 M urea, 2 M thiourea, 2% Chaps, 0.2% biolytes, 50 mM dithiothreitol, bromophenol blue dissolved in deionized water and made fresh before use). Samples were separated according to their isoelectric point using 11-cm, pH 3–10, immobilized pH gradient (IPG) strips, using an isoelectric focusing cell system (Bio-Rad) for the first-dimension separations. For each sample we produced two identical IPG strips with an equal amount of initial protein. After the proteins were separated in the first dimension, every pair of IPG strips was separated according to its molecular migration rate in one gel running box (each box ran two gels simultaneously) with precast Criterion XT 8–16% Bis–Tris gel w/Mops for the second-dimension separations. All gels ran under constant voltage (200 V) for 65 min. The "twin" gels from each sample were handled as follows: one twin gel was stained with Sypro ruby stain (Bio-Rad) for total protein and the second twin gel was

transferred to nitrocellulose and probed with the same antibodies/developer system as for the slot blots. Images of the twin spots from each couple (2D gel–HNE 2D blot) were processed with PDQuest 2-D analysis software (Bio-Rad) for each group to create master images. Optical densities of the master images for the individual spot signals were analyzed by calculating the average differences in the intensities between the gel spot and the corresponding HNE spot signal from the twin blot. Next, the ratiometric values were converted to a log scale and two-tailed *t* test, assuming unequal variances to identify the spots of the highest statistical significance. After all spots of interest were carefully mapped, gel plugs containing the selected proteins were cut. Each gel plug was trypsinized and peptides were cleaned with ZipTip (Millipore Corp., Bedford, MA, USA) procedures before the liquid chromatography–mass spectrometry analysis.

All mass spectra data reported in this study were acquired from the University of Louisville Mass Spectrometry Facility using nanospray ionization with tandem mass spectrometry (MS/MS) as described previously [21,22]. MS/MS spectra were searched against the International Protein Index (IPI) database using SEQUEST. IPI accession numbers were cross-correlated with SwissProt accession numbers for final protein identification.

Immunoprecipitation and immunoblotting

Animal heart tissues were homogenized with a chilled Teflon pestle in RIPA buffer (50 mM Tris–HCl, pH 7.9, 1% NP-40, 0.1% SDS, 150 mM NaCl, 1 mM EDTA, protease inhibitor cocktail, Calbiochem, Billerica, MA, USA), incubated for 30 min on ice, and then centrifuged for 10 min at 16,000 *g*. The supernatant containing 250 μg of protein in 0.5 ml RIPA buffer was precleaned with protein G-conjugated agarose beads (GE Healthcare, Cincinnati, OH, USA). HNE (2 μg), or mouse IgG antibody as control, was added. After overnight incubation at 4 °C, 40 μl of protein G-conjugated agarose beads was added and incubated for 1 h at 4 °C. The beads were washed four times with RIPA buffer and resuspended in 60 μl of Laemmli buffer. The immunoprecipitated samples were run on SDS–PAGE gels and blotted with specific antibodies at 1:1000 dilution. Western blots were prepared using the same protocol as described previously [23]. H9C2 cells were pretreated with 20 μM MnP for 1 h and then with 0.1 μM DOX and the same concentration of MnP for 3 days. The cell lysate was used for immunoprecipitation as described above.

Enzyme activity assays

ATP synthase and complex I activity was analyzed using the ATP synthase microplate kit and complex I activity kit (Abcam), respectively, following the manufacturer's protocols. Briefly, mitochondrial membrane proteins were isolated and immunocaptured in the wells of the microplate. The ATP synthase activity was measured by monitoring the conversion of ATP to ADP by ATP synthase coupled to the oxidation reaction of NADH to NAD^+ with a reduction in absorbance at 340 nm. The complex I activity was measured by following the oxidation of NADH to NAD^+ and the simultaneous reduction of a dye that leads to increased absorbance at 450 nm.

The DLD protein activity was measured by DLD-catalyzed NAD^+-dependent oxidation of dihydrolipoamide as described by Yan et al. [24]. Briefly, 2 μg of mitochondrial extract or 100 μg of cell lysate was mixed in 200 μl of total reaction volume with 100 mM potassium phosphate, pH 8.0, 1 mM EDTA, 0.6 mg/ml bovine serum albumin, and 3 mM NAD^+. The reaction was initiated by the addition of 3 mM dihydrolipoamide and measured at a wavelength 340 nm for 5 min.

SDHA activity was measured using a procedure [25,26] modified by our lab. Five micrograms of homogenized mitochondrial protein or 50 μg of H9C2 cellular protein in 200 μl of H_2O was mixed with 200 μl of reaction buffer (0.1 M potassium phosphate, pH 7.4, 0.1 M sodium succinate, 0.05 M sucrose) containing freshly added 1 mg/ml *p*-iodonitrotetrazolium violet (Sigma). The blank was prepared without sodium succinate. The reaction was incubated at 37 °C for 20 min, stopped with 400 μl of 5% trichloroacetic acid, and extracted with 0.8 ml of *N*-butanol. After centrifugation at 1000 rpm for 5 min, 200 μl of the upper layer was transferred to a 96-well plate and measured at OD 490 nm.

Mitochondrial function measurements

Oxygen consumption in cells and mitochondria was determined using the Seahorse extracellular flux (XF-96) analyzer (Seahorse Bioscience, Chicopee, MA, USA). To allow comparison between experiments, data are presented as oxygen consumption rate (OCR) in pmol/min/mg protein and extracellular acidification rate (ECAR) in mpH/min/mg protein. H9C2 cells were treated with various concentrations of DOX or saline for 48 h, trypsinized, and reseeded at 45,000 cells per well in triplicate under the same treatment conditions used in the Seahorse Bioscience XF microplates with glucose. After 24 h, basal OCR was measured four times and plotted as a function of cells under the basal condition followed by the sequential addition of oligomycin (1 μg/ml), FCCP (1 μM), antimycin (2 μM), and rotenone (1 μM), as indicated. Freshly isolated mitochondrial samples were plated at 3 μg per well in triplicate and immediately measured using the Seahorse analyzer. The progress curve is annotated to show the relative contributions of basal, ATP-linked, and maximal oxygen consumption after the addition of FCCP and the reserve capacity of the samples.

For the ECAR measurements, cells were washed and resuspended in assay medium lacking glucose. Basal ECAR was measured four times and plotted as a function of cells under basal conditions followed by the sequential addition of glucose (25 mM), oligomycin (1 μg/ml), and 2-deoxyglucose (2-DG; 25 mM), as indicated. The progress curve is annotated to show the relative contributions of glycolysis, glycolytic capacity, and glycolytic reserve of the cells.

WST and dichlorofluorescein (DCF) assays

Cells were plated at 6000/well or 2500/well for DCF or WST, respectively, in a 96-well plate, and pretreated with either 20 μM MnP or 1 mM NAC for 1 h, followed by treatment with either 0.1 or 0.25 μM DOX and the same concentration of MnP or NAC for 3 days (WST assay) or 1 h (DCF assay). WST assays were performed by following the manufacturer's instructions (Biovision, Mountain View, CA, USA). DCF assays were performed as previously described [27]. Briefly, after treatment, cells were incubated with 10 μg/ml carboxy-2′,7′-dichlorodihydrofluorescin diacetate (carboxy-H_2DCFDA, sensitive to oxidation, Invitrogen) and 1 μg/ml oxidized carboxy-dichlorofluorescin diacetate (carboxy-DCFDA, insensitive to oxidation, Invitrogen) in phosphate-buffered saline/2% fetal bovine serum at 37 °C for 20 min. The fluorescence in cells preloaded with carboxy-H_2DCFDA was normalized to that in cells preloaded with carboxy-DCFDA (ratio of H_2DCFDA/DCFDA) to control for the cell number, dye uptake, and ester cleavage differences between different treatment groups.

Statistical analysis

The samples used for 2D gel analysis, total HNE-adducted protein detection, and protein activity assays were $n \geq 6$. The experiments were conducted at least three times to verify the

reproducibility of the findings. Statistical analyses were carried out with Statistical Analysis System software (SAS Institute, Cary, NC, USA) and *P* values were calculated using the Student *t* test.

Results

Quantification of total HNE-bound protein and detection of specific proteins adducted by HNE in mitochondria

We isolated mitochondria from 9-week-old male C57BL/6 mice at 72 h after a single injection of DOX at 20 mg/kg ($n \geq 6$). First, we checked the expression of the total HNE-adducted protein in mitochondria by using a slot-blot apparatus and blotting with HNE antibody. The results showed that the total HNE-bound protein level was significantly increased, by 70.4%, in the mitochondria from mice treated with DOX vs saline (Fig. 1).

The same samples were used for detection of individual HNE-adducted proteins by 2D gel analysis (saline or DOX treated, $n = 6$). Each sample was separated using two 2D gels. One set of the gels was stained for visualization and quantification of proteins and the other was transferred onto nitrocellulose and was immune-detected with HNE antibody (Fig. 2). The specific HNE level for each protein was calculated as the ratio of the HNE level on the membrane to the protein level on the gel. Eight spots with the biggest average difference between saline and DOX treatments were identified, excised, and analyzed by mass spectrometry. As illustrated in Table 1, the mass spectrometry-identified proteins were ATP synthase subunit β (ATP5B), DLD, SDHA, NDUFS2, FH, trifunctional enzyme subunit α (HADHA), creatine kinase S-type (CKMT2), and 3-oxoacid–CoA transferase 1 (Oxct1).

Under basal aerobic conditions, heart muscle gets 60% of its energy from fat, 35% from carbohydrates, and 5% from amino acids and ketone bodies [28]. Among the identified proteins, HADHA is a subunit of the mitochondrial trifunctional protein, which catalyzes the last three steps of mitochondrial β-oxidation of long-chain fatty acids. Octx1 plays a central role in ketone body catabolism by catalyzing the reversible transfer of coenzyme A from succinyl-CoA to acetoacetate. CKMT2 is responsible for the transfer of high-energy phosphate from mitochondria to the cytosolic carrier creatine. The HADHA protein has been reported as being modified by HNE in the ventilator muscles of rats after lipopolysaccharide

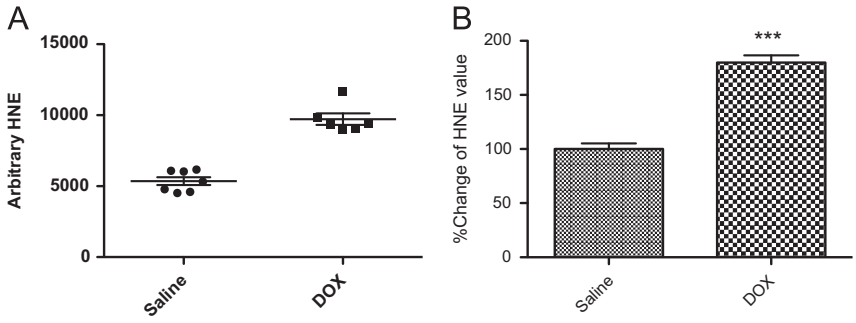

Fig. 1. Total HNE-adducted protein is significantly increased in mouse mitochondrial homogenate 3 days after DOX injection. (A) Absolute values of HNE-bound protein levels by slot-blot gel analysis. Mice were treated with DOX at 20 mg/kg for 3 days ($n \geq 6$). (B) The normalized % increase in HNE-adducted protein in DOX-treated vs saline-treated mice. $^{***}P < 0.0001$ compared with samples from saline-treated mice.

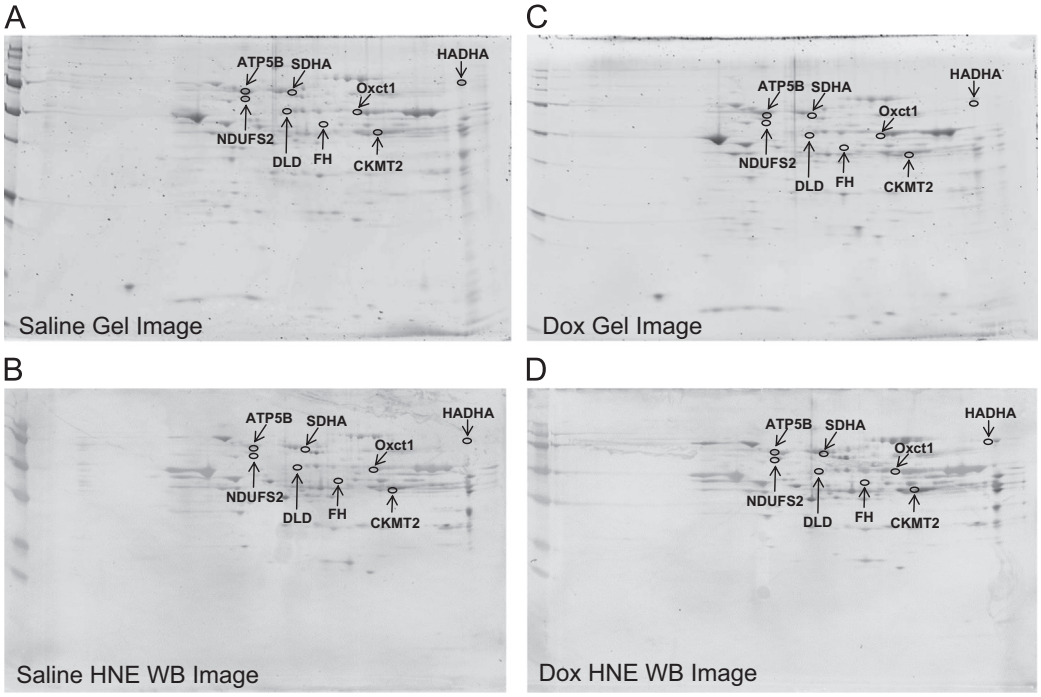

Fig. 2. HNE-adducted proteins identified by redox proteomics. (A and C) Representative 2D gels and (B and D) corresponding 2D HNE Western blot images from saline-treated (A and B) or DOX-treated (C and D) mice ($n = 6$). The protein spots identified are circled and labeled.

Table 1
Mouse mitochondrial cardiac proteins showing increased HNE levels at 3 days after DOX injection.

Protein identified	Accession No.	Coverage	No. of peptides[a]	Score	MW (kDa)	pI	*t* test	Fold change[b]
ATP synthase subunit β	P56480	17.6	6	31.0	56.3	5.34	0.036	10.9
Dihydrolipoyl dehydrogenase	O08749	22.2	9	57.8	54.2	7.90	0.054	8.94
Succinate dehydrogenase [ubiquinone] flavoprotein subunit	Q8K2B3	15.7	6	42.3	72.5	7.37	0.057	7.20
Trifunctional enzyme subunit α	Q8BMS1	24.0	16	137	82.6	9.14	0.038	4.97
Creatine kinase S-type	Q6P8J7	41.0	13	118	47.4	8.40	0.051	4.40
Cytoplasmic isoform of fumarate hydratase	P97807-2	12.4	4	27.1	50.0	7.94	0.029	3.66
Succinyl-CoA:3-ketoacid–coenzyme A transferase 1	Q3UJQ9	15.8	4	12.5	52.2	8.94	0.057	3.46
NADH dehydrogenase [ubiquinone] iron–sulfur protein 2	Q91WD5	48.0	16	145	52.6	6.99	0.058	1.98

[a] The number of peptide sequences identified by nanospray ESI–MS/MS of tryptic peptides.
[b] The fold change in spot density from DOX-treated compared with saline-treated.

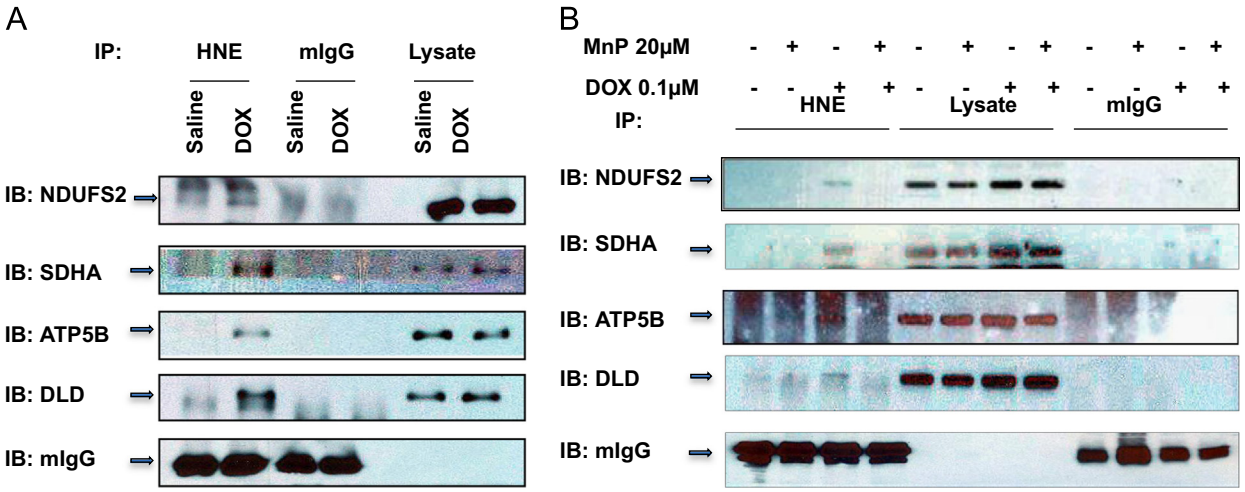

Fig. 3. Immunoprecipitation of HNE-adducted proteins. (A) Murine heart homogenates from mice treated with either saline or DOX for 3 days were immunoprecipitated with mouse HNE antibody (lanes 1 and 2) or mouse IgG antibody (lanes 3 and 4) as control. 20 μg of total heart homogenates from immunoprecipitated (IP) samples was loaded in lanes 5 and 6. The immunoprecipitates were immunoblotted (IB) with antibodies specific for the indicated proteins. The experiment was repeated three times to verify the results. (B) H9C2 cells were pretreated with 20 μM MnP followed with 0.1 μM DOX and MnP for 3 days. 500 μg of cell lysate was used for each immunoprecipitation. Lanes 1–4 are immunoprecipitations with mouse HNE antibody, lanes 5–8 are 20 μg of each cell lysate, and lanes 9–12 are immunoprecipitations with mouse IgG antibody.

(LPS) induction [29] and its function was reduced after DOX treatment in rat and mouse [30,31]. Interestingly, the other five proteins directly participate in the TCA cycle, a system critical for the maintenance of cardiomyocyte function [32,33]. Therefore, in this study we focused on the five TCA cycle component proteins.

Verification of HNE adduction by immunoprecipitation and examination of expression levels of the HNE-adducted proteins by Western blot analysis

To verify HNE adduction to the proteins, we performed immunoprecipitation with HNE antibody followed by Western blot analysis with specific antibodies to each of the five proteins. In these experiments, we used whole-heart homogenates from mice treated with saline or DOX for 3 days. The data demonstrate that ATP5B, DLD, SDHA, and NDUFS2 were immunoprecipitated by HNE antibody but not by the control IgG antibody (Fig. 3A). However, we were unable to immunoprecipitate FH protein with HNE antibody (data not shown). Our results confirm that ATP5B, DLD, SDHA, and NDUFS2 were modified by HNE.

To further verify whether HNE adduction of the proteins is due to DOX-induced ROS, we performed immunoprecipitation on H9C2 cells treated with DOX in the presence or absence of 20 μM MnP. MnP is an optimized superoxide dismutase (SOD) mimetic, which mimics well the thermodynamics and kinetics of the catalysis of superoxide dismutation by SOD. It further is a lipophilic analog that has enhanced mitochondrial accumulation, but reduced cellular toxicity [34–37]. As shown in Fig. 3B, the MnP treatment protected the proteins from HNE adduction.

To investigate whether DOX treatment would alter the expression level of the four identified proteins, Western blot analysis was performed on mouse whole-heart homogenates as well as mitochondrial homogenates. As demonstrated in Fig. 4A, the protein expression levels were not affected by DOX treatment in either whole heart or mitochondrial homogenates. To further verify the results, we performed Western blot analysis on H9C2 cell extracts (Fig. 4B). The cells were treated with 0.1 or 0.25 μM DOX for 72 h. Our H9C2 data support the finding that DOX treatment did not change the expression levels of the proteins in mice.

Examination of enzyme activity

HNE modification of proteins often leads to altered protein activity [38,39]. Therefore, we next checked the activity of the individual proteins.

Mammalian mitochondrial complex I is composed of at least 43 different subunits. The NDUFS2 subunit is the third largest subunit, located in the extramembranous part of complex I, near the membrane domain [40]. Disruption of this subunit results in the complete absence of the peripheral arm of complex I and in mitochondrial complex I deficiency [40]. Because the NDUFS2 subunit is a component of complex I, we measured the complex

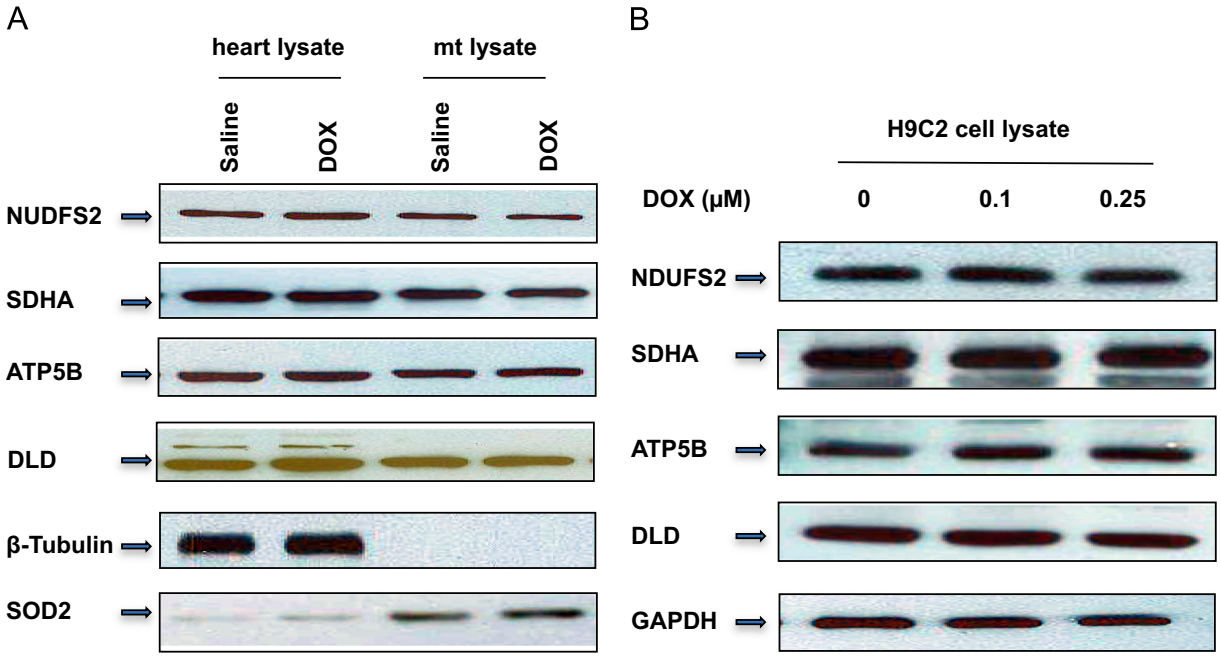

Fig. 4. Western blot analysis of the identified HNE-adducted proteins. (A) 30 μg of total mouse heart homogenate and 10 μg of mouse mitochondrial homogenate from 3-day DOX-treated mice were loaded in gels and blotted with various antibodies as indicated. β-Tubulin and SOD2 were used as total heart homogenate and mitochondrial fraction loading controls, respectively. (B) Total H9C2 cell extracts treated with the indicated concentrations of DOX for 3 days were loaded and blotted with indicated antibodies. The experiments were repeated four times.

I activity. The level of complex I activity was reduced by 36% in mouse mitochondrial homogenates after DOX treatment and 77% in H9C2 cell extracts with 0.1 μM DOX treatment. The reduced activity in H9C2 cells treated with DOX was dose dependent (data not shown).

SDHA encodes a major catalytic subunit of succinate-ubiquinone oxidoreductase in complex II located in the inner mitochondrial membrane. It also participates in the TCA cycle, catalyzing succinate to fumarate conversion. Our results show that the SDHA activity in mouse heart mitochondrial homogenates and H9C2 cell extracts dropped 17.4 and 51.8%, respectively, after DOX treatment (Fig. 5B).

ATP synthase subunit β is an enzyme encoded by the *ATP5B* gene, one of the five subunits in the catalytic portion of complex V. The enzyme synthesizes ATP from ADP in the presence of a proton gradient across the mitochondrial inner membrane generated by the electron transport chain. In this experiment, we used the ELISA-based ATP synthase activity kit, which first captures the ATP synthase complex in the reaction wells and then measures the activity by oxidation of NADH to NAD^+. Our measurements show that ATP synthase activity was reduced by 27.4% in H9C2 cells treated with DOX and 44% in mitochondrial homogenates (Fig. 5C).

DLD is a flavoprotein encoded by the *DLD* gene. The enzyme is a component in the α-ketoglutarate dehydrogenase complex, which catalyzes the decarboxylation of α-ketoglutarate into succinyl-CoA in the TCA cycle, and the pyruvate dehydrogenase complex, which catalyzes pyruvate to acetyl-CoA before the TCA cycle. The DLD activity was determined by measuring NAD^+-dependent oxidation of dihydrolipoamide [24]. We used heart mitochondrial homogenates and H9C2 cell extracts treated with saline or DOX. The activity of DLD was reduced by 28.5 and 75.1%, respectively (Fig. 5D).

Examination of mitochondrial function

Our results show that DOX treatment reduced the activities of several enzymes in the TCA cycle. To determine whether HNE adduction of the proteins in mitochondrial complexes is related to mitochondrial dysfunction, we examined mitochondrial function by using a Seahorse extracellular flux (XF-96) analyzer. We assessed OCR on isolated crude mitochondria from mice, as well as OCR and ECAR from H9C2 cells treated with DOX.

OCR measures oxygen-dependent mitochondrial respiration. Oligomycin injections inhibit ATP synthesis by blocking ETC complex V, which distinguishes the oxygen consumption devoted to ATP synthesis from the oxygen consumption required to overcome the natural proton leak across the inner mitochondrial membrane. The injection of FCCP decouples ATP synthesis and hydrogen ion transport, leading to rapid consumption of energy and oxygen (mitochondrial maximal capacity) without the generation of ATP. FCCP treatment is also used to calculate the reserve oxygen consumption capacity of mitochondria under stress conditions [32,41]. The reserve capacity was calculated with the difference between maximal OCR and basal OCR. Rotenone and antimycin were used to inhibit the function of complexes I and III, respectively. The application of the two drugs completely inhibited the function of the ETC.

These experiments used freshly isolated mouse mitochondria after 3-day treatment with DOX and H9C2 cells treated with DOX for 3 days. The results showed reduced basal oxygen consumption that was consistent with our discovery of damaged complex I. As expected, the significantly reduced OCR in ATP-linked maximal capacity as well as reserve capacity after DOX treatment supports our findings of deficiency in complex II and V activities (Fig. 6A and B). The DOX effect was dose dependent in H9C2 cells. As shown in Fig. 6C, treating mice with MnP prevented DOX-induced damage in mitochondrial respiration.

ECAR measures extracellular acidification rate generated from glycolysis independent of oxygen. We also assessed the differences in glycolysis-induced ECAR among the samples. The measurement after injection of oligomycin represents glycolytic reserve. The injection of 2-DG, a glycolysis inhibitor, shut down the entire glycolytic process. The results of extracellular proton flux reveal that DOX-treated H9C2 cells showed a significant increase in extracellular acidification rates in glycolysis and glycolytic reserve (Fig. 6D), suggesting that these cells exhibited enhanced glycolysis.

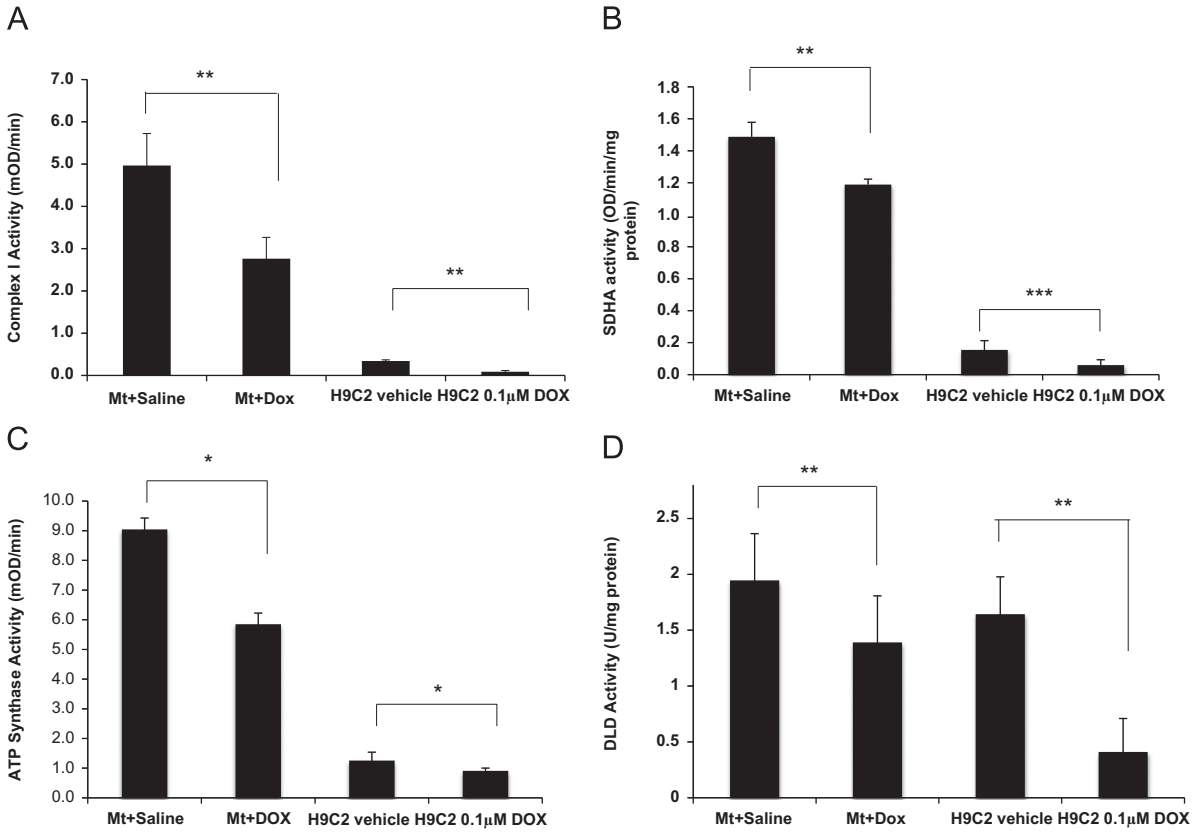

Fig. 5. Enzymatic activity of mitochondrial complex I, SDHA, ATP synthase, and DLD. Mitochondrial homogenates or H9C2 cell extracts treated with saline or DOX ($n = 6$ mice, cells repeated at least three times) were used. The amounts of protein from mitochondrial homogenates or H9C2 extracts used for each reaction in different assays were as follows: complex I, 20 or 100 μg; SDHA, 5 or 50 μg; DLD, 2 or 50 μg; ATP synthase, 0.5 or 100 μg; respectively. (A, B, C, D) The activity for complex I, SDHA, ATP synthase, or DLD, respectively. Mt represents mitochondrial homogenate. Data are expressed as the mean ± SD. $P < 0.05$ was considered significant (Student's t test). $^{*}P < 0.05$; $^{**}P < 0.01$; $^{***}P < 0.001$ as compared with controls.

Assessment of ROS generation by treatment of DOX with or without two different classes of redox-active compounds

Elevated ROS in cells is considered one of the major mechanisms of DOX-induced toxicity. HNE is one of the most active lipid peroxidation products generated via ROS- mediated injury. We next did a DCF assay to check the ROS levels in DOX-treated H9C2 cells in the presence or absence of antioxidants. As shown in Fig. 7A, 0.1 or 0.25 μM DOX treatment rapidly (after 1 h) induced normalized carboxy-H_2DCFDA fluorescence, a general indicator of cellular ROS level. Moreover, MnP or NAC treatment significantly reduced cellular ROS level upon DOX treatment. Our results also suggest that DOX-induced elevation of cellular ROS is a relatively early event.

Cardiomyocytes have a high number of mitochondria and their function depends heavily on mitochondrial respiration. We next did a WST assay to determine the survival of H9C2 cells treated with DOX with or without antioxidants. The results show (Fig. 7B) that 20 μM MnP or 1 mM NAC partially but significantly protected the survival of H9C2 cells treated with DOX at 0.25 μM concentration. However, MnP, but not NAC, significantly reduced cardiomyocyte death at lower DOX concentrations. These results suggest that redox-active compounds, able to reduce levels of reactive species via their antioxidative actions, play an important role in the attenuation of DOX-induced toxicity in vitro.

Discussion

This study is the first global approach to identify specific HNE-adducted proteins associated with the TCA cycle and ETC chain after DOX treatment in mice. We chose to use a single high dose (20 mg/kg) of DOX, which is equivalent to a high-dose single injection in cancer patients, such as those with small-cell lung cancer [42], and has been used in a variety of animal models [23,43,44]. In our previous studies, we observed mitochondrial ultrastructural damage 5 days after this treatment [45]. Rosenoff et al. [43] also reported cardiomyopathy in mice 4 days after this dosage, which is similar to the delayed DOX-induced cardiomyopathy noted in humans.

At least 20% of cardiomyocyte volume is composed of mitochondria in human and 32% in mouse [46,47], enabling efficient energy production via oxidative phosphorylation. At basal metabolic rates, more than 95% of energy that sustains cardiac function and viability is derived from aerobic metabolism [28]. Damaged oxidative phosphorylation in mitochondria can lead to reliance on anaerobic glycolysis, which may provide a short-term solution, but prolonged dependence most likely results in a severe energy deficiency that ultimately creates a bioenergetics crisis and leads to cardiac failure [14].

Our data are consistent with those observed for the HNE adduction of proteins in diabetes and cardiovascular diseases, such as ischemic heart and congestive heart failure [48–50]. It has been reported that treatment of isolated crude animal mitochondria by HNE induces mitochondrial respiration deficiency [41,49–51]. HNE modification of SDHA [52], DLD [29], and ATP5B [53] as well as NDUFS2 [54] has been identified in vitro or in vivo under oxidative conditions by various researchers. However, the exact proteins modified by HNE in mitochondrial respiration after DOX or HNE treatment have not been reported. Using global analysis, we found that several major HNE-adducted proteins were involved in the TCA cycle and ETC (Fig. 8). In addition, we show that the activities of complexes I, II, and V were decreased by DOX. Furthermore, our bioenergetics results

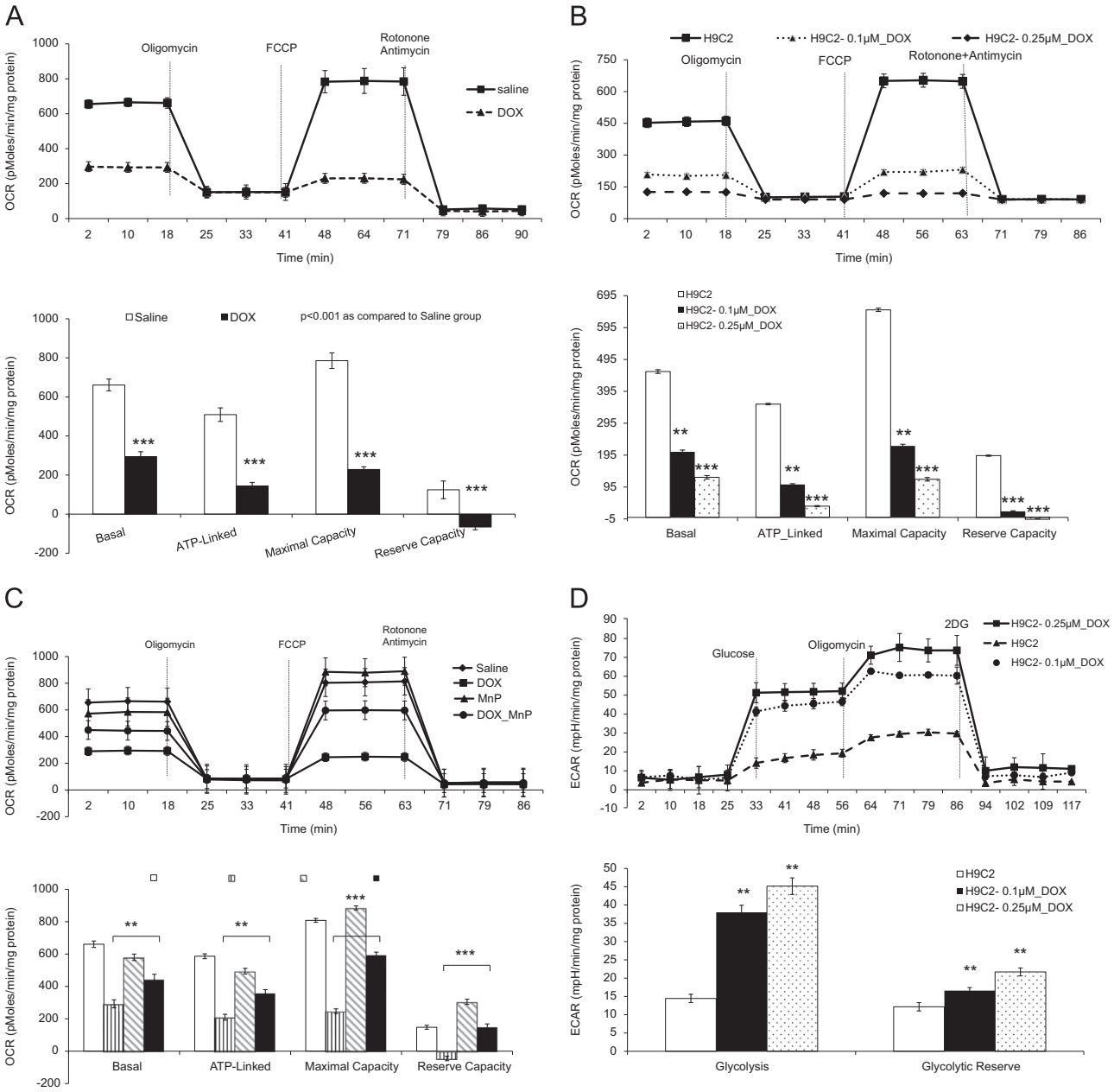

Fig. 6. Oxygen consumption rate (OCR) and extracellular acidification rate (ECAR) in mouse mitochondria and H9C2 cells. The Seahorse XF96 analyzer in the presence of mitochondrial inhibitors (oligomycin 1 μg/ml, FCCP 1 μM, or rotenone 1 μM and antimycin 2 μM) was used in the assays for OCR and ECAR. (A) The OCR of mitochondria freshly isolated from mouse heart at 3 days after saline or DOX injection. The units (pmol/min/mg protein) for basal OCR, ATP-linked oxygen consumption, maximum OCR after addition of FCCP, and reserve capacity of the cells were calculated and plotted. (B) The OCR of H9C2 cells after 3 days saline or DOX treatment and corresponding quantitation. (C) The OCR of H9C2 cells pretreated with MnP for 1 h and 3 days treatment with DOX together with MnP. (D) ECAR of H9C2 cells with the same treatment as for (B). Cells were cultured for 2 h in the absence of glucose. Three sequential injections of D-glucose (2 g/L), oligomycin (1 μM), and 2-deoxyglucose (100 mM) provided ECAR associated with glucose consumption. Glycolysis was defined as ECAR after the addition of D-glucose. The glycolytic capacity, defined as ECAR after the addition of oligomycin, and glycolytic reserve capacity, defined as the difference in ECAR after the addition of oligomycin after the addition of 2-DG, were calculated and plotted.

demonstrate that mitochondrial oxidative respiration was severely damaged and glycolysis was increased after DOX treatment, suggesting a shift of energy production in the damaged hearts.

Mitochondrial complex I is a multisubunit protein complex and an entry point for electrons into the respiratory chain in mitochondria. Mutations of the *NDUFS2* gene are associated with mitochondrial complex I deficiency and cardiomyopathy [55]. Complex I is also a major source of cellular ROS and one of the three major DOX metabolism pathways [56]. The semiquinone to quinone cycling of DOX is carried out in complex I, which leads to the formation of superoxide and other ROS products [14,57]. This laboratory and others have reported decreased complex I activity after DOX treatment [4,44,58,59]. Our current results extend these findings and demonstrate, for the first time, that the NUDSF2 subunit is adducted by HNE after DOX treatment, suggesting that this adduction may be a cause of DOX-induced complex I deficiency. There are seven Fe–sulfur protein subunits in mitochondrial complex I. The differential susceptibility of these proteins to oxidative modification upon DOX treatment is not clear. NUDSF2 and NUDFS7 are the membrane-proximal subunits of the seven and the last proteins in the electron transport sequence in complex I. It is possible that the relative positions of these Fe–sulfur proteins to the membrane may play a role in modification by a lipid peroxidation product such as HNE.

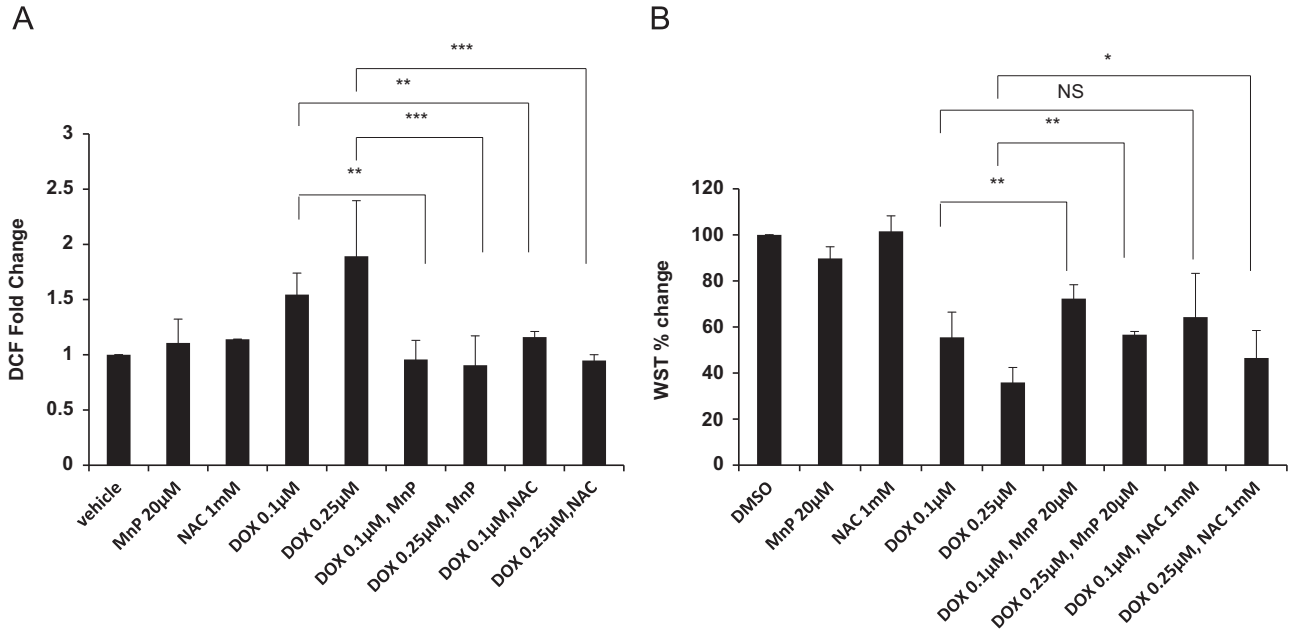

Fig. 7. DCF and WST assays on H9C2 cells. (A) The fold change of DCF in H9C2 cells pretreated with MnP or NAC for 1 h and then treated with DOX/MnP or NAC for 1 h. (B) The % change of WST in H9C2 cells pretreated with MnP or NAC for 1 h and then treated with DOX/MnP or NAC for 3 days. $^{*}P < 0.05$; $^{**}P < 0.01$; $^{***}P < 0.001$ as compared with samples from DOX treated.

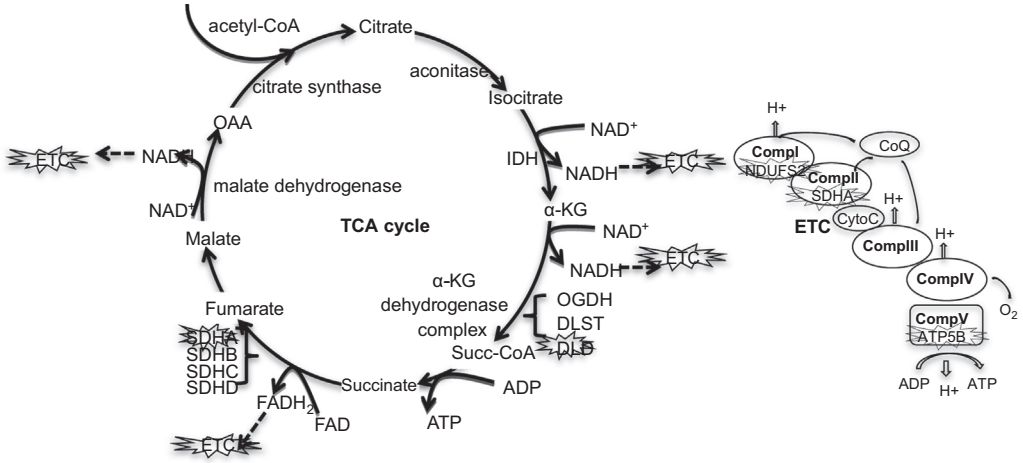

Fig. 8. A schematic demonstration of the identified HNE-adducted proteins in the TCA cycle and ETC. The main steps in the TCA cycle and ETC are presented. The HNE-adducted and functionally affected proteins are marked.

SDHA is one of the four subunits in ETC complex II and participates in the TCA cycle to catalyze succinate to fumarate conversion. Lashin et al. [60] have reported that complex II activity was reduced in diabetic rat hearts and identified one of the subunits in complex II as having been modified by HNE. Defects in SDHA cause cardiomyopathy dilated type 1GG (CMD1GG) [61]. CMD1GG is a disorder characterized by ventricular dilation and impaired systolic function, resulting in congestive heart failure, which shares a pathology similar to DOX-induced cardiac damage. Our previous study in DOX-treated mouse heart tissue also demonstrates a decline in complex II activity after DOX treatment, but the protein responsible for the defective complex II activity was unknown. In the current study, we identify SDHA as a HNE-modified protein in complex II, suggesting that HNE adduction of SDHA may contribute to the reduced function of complex II in both mouse mitochondria and H9C2 cells treated with DOX.

ATP synthase/complex V synthesizes ATP from ADP by phosphorylation in the presence of oxygen and a proton gradient across the membrane. Complex V is composed of two structural domains, F(1), which contains the extramembranous catalytic core, and F(0), which contains the membrane proton channel. ATP5B is one of the five subunits in F(1). DOX has been shown to inhibit the F0F1 proton pump of mitochondria [62,63], but the exact target for the effect of DOX remains unknown. In this study, we demonstrate that ATP5B is adducted by HNE and that ATP synthase complex activity was reduced after DOX treatment, suggesting ATP5B to be the target for DOX-mediated inactivation of F0F1 function.

DLD is a component of the pyruvate dehydrogenase complex (catalyzing pyruvate to acetyl-CoA), the α-ketoglutarate dehydrogenase complex (catalyzing α-ketoglutarate to succinate) in the TCA cycle, and the branched-chain α-keto acid dehydrogenase complex (involved in the breakdown of amino acids—leucine, isoleucine, and valine). The enzyme is redox sensitive [24] and has two redox-reactive cysteine residues at its active center that are indispensable for its catalytic function [64]. It has been reported that DLD was modified by HNE in the ventilatory muscles of rats after LPS treatment [29]. Our finding that HNE adduction of DLD is associated with the impaired activity of this protein is

consistent with the decline in oxidative metabolism of cardiac tissue after DOX treatment.

In our mitochondrial function study, the oxygen consumption rate was significantly reduced by DOX. It is worth mentioning that our data demonstrate that DOX reduces basal oxygen consumption, which differs from other reports showing that stress overload as well as ischemia in isolated cardiomyocytes results in increased basal oxygen consumption [65]. However, this reduction is consistent with the DOX-induced damage to complex I and defective ETC activity. Thus, stress overload and DOX-induced effect might have different outcomes.

DOX, though an older chemotherapeutic drug, remains in active use for cancer treatments, despite its known cardiac toxicity, because of its therapeutic efficacy [1]. Although attempts have been made to develop newer analogs that are less cardiotoxic, the resulting products are not as efficient as DOX [1]. Thus, identification of selective targets in DOX-induced cardiotoxicity may lead to potential therapeutic interventions. In addition to DOX, nearly 50% of the current FDA-approved anticancer drugs are known to generate ROS [66]. Thus, the cardiovascular side effects of DOX may share common mechanisms with other anticancer drugs known to cause cardiac injury. We and others have previously shown that overexpression of antioxidant enzymes, such as manganese superoxide dismutase [45] and catalase [67], can protect the heart from DOX cardiotoxicity in transgenic mice. It should also be noted that, whereas DOX causes oxidative stress via redox cycling of its quinone moiety and the consequent accumulation of ROS is well documented, it has been shown recently that DOX-induced DNA double-strand breaks by poisoning of topoisomerase 2β and transcriptome changes are responsible for defective mitochondrial biogenesis and ROS formation regardless of anthracycline redox cycling [68]. Thus, it is possible that the lipid peroxidation and protein adduction caused by HNE might be both the determinants and the consequences of mitochondrial dysfunction and cardiotoxicity. However, our DCF results show that DOX-induced ROS increase is rather an early event. Although classical antioxidants and ROS scavengers (such as NAC and vitamin E), usually very effective in acute DOX cardiotoxicity experiments, have failed in clinical trials, there were discrepancies in the concentrations/doses of antioxidants used in vitro and in vivo as well as their local concentrations in mitochondria [69]. Thus, the redox-active compounds, which, like MnP, efficiently accumulate in mitochondria and are powerful scavengers of reactive species [70] should be considered for future clinical studies. The data obtained from this study provide specific markers for identifying and testing the cardioprotective effect of various antioxidants, mimetics, or agents that selectively protect against DOX-induced cardiac injury and would benefit a large number of patients.

Acknowledgments

This work is supported by NIH Grants CA 049797 and CA 139843, Cancer Center Support Grant (CCSG) P30CA177558 from the NCI, and the Edward P. Evans Foundation. The authors thank the University of Kentucky Free Radical Biology in Cancer Shared Resource Facility for its support. We also thank Dr. Liang-Jun Yan of the University of North Texas Health Science Center for the kind gift of synthesized dihydrolipoamide, as well as for his excellent technical help.

Appendix A. Supplementary material

Supplementary data associated with this article can be found in the online version at http://dx.doi.org/10.1016/j.freeradbiomed.2014.03.001.

References

[1] Pang, B.; Qiao, X.; Janssen, L.; Velds, A.; Groothuis, T.; Kerkhoven, R.; Nieuwland, M.; Ovaa, H.; Rottenberg, S.; van Tellingen, O.; Janssen, J.; Huijgens, P.; Zwart, W.; Neefjes, J. Drug-induced histone eviction from open chromatin contributes to the chemotherapeutic effects of doxorubicin. *Nat. Commun.* **4:**1908; 2013.

[2] Chatterjee, K.; Zhang, J.; Honbo, N.; Karliner, J. S. Doxorubicin cardiomyopathy. *Cardiology* **115:**155–162; 2010.

[3] Singal, P. K.; Iliskovic, N. Doxorubicin-induced cardiomyopathy. *N. Engl. J. Med.* **339:**900–905; 1998.

[4] Marcillat, O.; Zhang, Y.; Davies, K. J. Oxidative and non-oxidative mechanisms in the inactivation of cardiac mitochondrial electron transport chain components by doxorubicin. *Biochem. J.* **259:**181–189; 1989.

[5] Minotti, G.; Recalcati, S.; Mordente, A.; Liberi, G.; Calafiore, A. M.; Mancuso, C.; Preziosi, P.; Cairo, G. The secondary alcohol metabolite of doxorubicin irreversibly inactivates aconitase/iron regulatory protein-1 in cytosolic fractions from human myocardium. *FASEB J.* **12:**541–552; 1998.

[6] Stadtman, E. R.; Berlett, B. S. Reactive oxygen-mediated protein oxidation in aging and disease. *Chem. Res. Toxicol.* **10:**485–494; 1997.

[7] Yang, Y.; Sharma, R.; Sharma, A.; Awasthi, S.; Awasthi, Y. C. Lipid peroxidation and cell cycle signaling: 4-hydroxynonenal, a key molecule in stress mediated signaling. *Acta Biochim. Pol.* **50:**319–336; 2003.

[8] Porta, E. A.; Joun, N. S.; Matsumura, L.; Nakasone, B.; Sablan, H. Acute adriamycin cardiotoxicity in rats. *Res. Commun. Chem. Pathol. Pharmacol.* **41:**125–137; 1983.

[9] al-Shabanah, O. A.; Badary, O. A.; Nagi, M. N.; al-Gharably, N. M.; al-Rikabi, A. C.; al-Bekairi, A. M. Thymoquinone protects against doxorubicin-induced cardiotoxicity without compromising its antitumor activity. *J. Exp. Clin. Cancer Res.* **17:**193–198; 1998.

[10] Perluigi, M.; Coccia, R.; Butterfield, D. A. 4-Hydroxy-2-nonenal, a reactive product of lipid peroxidation, and neurodegenerative diseases: a toxic combination illuminated by redox proteomics studies. *Antioxid. Redox Signaling* **17:**1590–1609; 2012.

[11] Zhou, L.; O'Rourke, B. Cardiac mitochondrial network excitability: insights from computational analysis. *Am. J. Physiol. Heart Circ. Physiol.* **302:**H2178–H2189; 2012.

[12] Goormaghtigh, E.; Huart, P.; Praet, M.; Brasseur, R.; Ruysschaert, J. M. Structure of the adriamycin–cardiolipin complex: role in mitochondrial toxicity. *Biophys. Chem.* **35:**247–257; 1990.

[13] Davies, K. J.; Doroshow, J. H. Redox cycling of anthracyclines by cardiac mitochondria. I. Anthracycline radical formation by NADH dehydrogenase. *J. Biol. Chem.* **261:**3060–3067; 1986.

[14] Berthiaume, J. M.; Wallace, K. B. Adriamycin-induced oxidative mitochondrial cardiotoxicity. *Cell Biol. Toxicol.* **23:**15–25; 2007.

[15] Grimsrud, P. A.; Xie, H.; Griffin, T. J.; Bernlohr, D. A. Oxidative stress and covalent modification of protein with bioactive aldehydes. *J. Biol. Chem.* **283:**21837–21841; 2008.

[16] Carvalho, F. S.; Burgeiro, A.; Garcia, R.; Moreno, A. J.; Carvalho, R. A.; Oliveira, P. J. Doxorubicin-induced cardiotoxicity: from bioenergetic failure and cell death to cardiomyopathy. *Med. Res. Rev.* **34:**106–135; 2014.

[17] Lefrak, E. A.; Pitha, J.; Rosenheim, S.; Gottlieb, J. A. A clinicopathologic analysis of adriamycin cardiotoxicity. *Cancer* **32:**302–314; 1973.

[18] Green, P. S.; Leeuwenburgh, C. Mitochondrial dysfunction is an early indicator of doxorubicin-induced apoptosis. *Biochim. Biophys. Acta* **1588:**94–101; 2002.

[19] Velez, J. M.; Miriyala, S.; Nithipongvanitch, R.; Noel, T.; Plabplueng, C. D.; Oberley, T.; Jungsuwadee, P.; Van Remmen, H.; Vore, M.; St Clair, D. K. p53 regulates oxidative stress-mediated retrograde signaling: a novel mechanism for chemotherapy-induced cardiac injury. *PLoS One* **6:**e18005; 2011.

[20] Reed, T.; Perluigi, M.; Sultana, R.; Pierce, W. M.; Klein, J. B.; Turner, D. M.; Coccia, R.; Markesbery, W. R.; Butterfield, D. A. Redox proteomic identification of 4-hydroxy-2-nonenal-modified brain proteins in amnestic mild cognitive impairment: insight into the role of lipid peroxidation in the progression and pathogenesis of Alzheimer's disease. *Neurobiol. Dis.* **30:**107–120; 2008.

[21] Jungsuwadee, P.; Cole, M. P.; Sultana, R.; Joshi, G.; Tangpong, J.; Butterfield, D. A.; St Clair, D. K.; Vore, M. Increase in Mrp1 expression and 4-hydroxy-2-nonenal adduction in heart tissue of adriamycin-treated C57BL/6 mice. *Mol. Cancer Ther.* **5:**2851–2860; 2006.

[22] Fiorini, A.; Sultana, R.; Forster, S.; Perluigi, M.; Cenini, G.; Cini, C.; Cai, J.; Klein, J. B.; Farr, S. A.; Niehoff, M. L.; Morley, J. E.; Kumar, V. B.; Allan Butterfield, D. Antisense directed against PS-1 gene decreases brain oxidative markers in aged senescence accelerated mice (SAMP8) and reverses learning and memory impairment: a proteomics study. *Free Radic. Biol. Med.* **65C:**1–14; 2013.

[23] Chen, Y.; Daosukho, C.; Opii, W. O.; Turner, D. M.; Pierce, W. M.; Klein, J. B.; Vore, M.; Butterfield, D. A.; St Clair, D. K. Redox proteomic identification of oxidized cardiac proteins in adriamycin-treated mice. *Free Radic. Biol. Med.* **41:**1470–1477; 2006.

[24] Yan, L. J.; Sumien, N.; Thangthaeng, N.; Forster, M. J. Reversible inactivation of dihydrolipoamide dehydrogenase by mitochondrial hydrogen peroxide. *Free Radic. Res.* **47:**123–133; 2013.

[25] Pennington, R. J. Biochemistry of dystrophic muscle: mitochondrial succinate-tetrazolium reductase and adenosine triphosphatase. *Biochem. J.* **80:**649–654; 1961.

[26] Takiyyuddin, M. A.; Cervenka, J. H.; Hsiao, R. J.; Barbosa, J. A.; Parmer, R. J.; O'Connor, D. T. Chromogranin A: storage and release in hypertension. *Hypertension* **15:**237–246; 1990.

[27] Sun, Y.; St Clair, D. K.; Xu, Y.; Crooks, P. A.; St Clair, W. H. A NADPH oxidase-dependent redox signaling pathway mediates the selective radiosensitization effect of parthenolide in prostate cancer cells. *Cancer Res.* **70:**2880–2890; 2010.

[28] Barret, K. E.; Barman, S. M.; Boitano, S.; Brooks, H. L. *Ganong's Review of Medical Physiology*. 22nd edition. New York: McGraw–Hill; 2005.

[29] Hussain, S. N.; Matar, G.; Barreiro, E.; Florian, M.; Divangahi, M.; Vassilakopoulos, T. Modifications of proteins by 4-hydroxy-2-nonenal in the ventilatory muscles of rats. *Am. J. Physiol. Lung Cell. Mol. Physiol.* **290**; 2006. (L996-1003).

[30] Robison, T. W.; Giri, S. N.; Wilson, D. W. Effects of chronic administration of doxorubicin on myocardial creatine phosphokinase and antioxidant defenses and levels of lipid peroxidation in tissues and plasma of rats. *J. Biochem. Toxicol.* **4:**87–94; 1989.

[31] Mihm, M. J.; Coyle, C. M.; Schanbacher, B. L.; Weinstein, D. M.; Bauer, J. A. Peroxynitrite induced nitration and inactivation of myofibrillar creatine kinase in experimental heart failure. *Cardiovasc. Res.* **49:**798–807; 2001.

[32] Sansbury, B. E.; Jones, S. P.; Riggs, D. W.; Darley-Usmar, V. M.; Hill, B. G. Bioenergetic function in cardiovascular cells: the importance of the reserve capacity and its biological regulation. *Chem. Biol. Interact.* **191:**288–295; 2011.

[33] Bugger, H.; Guzman, C.; Zechner, C.; Palmeri, M.; Russell, K. S.; Russell 3rd R. R. Uncoupling protein downregulation in doxorubicin-induced heart failure improves mitochondrial coupling but increases reactive oxygen species generation. *Cancer Chemother. Pharmacol.* **67:**1381–1388; 2011.

[34] Rajic, Z.; Tovmasyan, A.; Spasojevic, I.; Sheng, H.; Lu, M.; Li, A. M.; Gralla, E. B.; Warner, D. S.; Benov, L.; Batinic-Haberle, I. A new SOD mimic, Mn(III) *ortho* *N*-butoxyethylpyridylporphyrin, combines superb potency and lipophilicity with low toxicity. *Free Radic. Biol. Med.* **52:**1828–1834; 2012.

[35] Adachi, K.; Fujiura, Y.; Mayumi, F.; Nozuhara, A.; Sugiu, Y.; Sakanashi, T.; Hidaka, T.; Toshima, H. A deletion of mitochondrial DNA in murine doxorubicin-induced cardiotoxicity. *Biochem. Biophys. Res. Commun.* **195:**945–951; 1993.

[36] Miriyala, S.; Spasojevic, I.; Tovmasyan, A.; Salvemini, D.; Vujaskovic, Z.; St Clair, D.; Batinic-Haberle, I. Manganese superoxide dismutase, MnSOD and its mimics. *Biochim. Biophys. Acta* **1822:**794–814; 2012.

[37] Batinic-Haberle, I.; Tovmasyan, A.; Roberts, E.R.; Vujaskovic, Z.; Leong, K.W.; Spasojevic I. SOD therapeutics: latest insights into their structure–activity relationships and impact on the cellular redox-based signaling pathways, *Antioxid. Redox Signaling*, http://dx.doi.org/10.1089/ars.2012.5147, in press.

[38] Gewirtz, D. A. A critical evaluation of the mechanisms of action proposed for the antitumor effects of the anthracycline antibiotics adriamycin and daunorubicin. *Biochem. Pharmacol.* **57:**727–741; 1999.

[39] Minotti, G.; Menna, P.; Salvatorelli, E.; Cairo, G.; Gianni, L. Anthracyclines: molecular advances and pharmacologic developments in antitumor activity and cardiotoxicity. *Pharmacol. Rev.* **56:**185–229; 2004.

[40] Gianni, L.; Herman, E. H.; Lipshultz, S. E.; Minotti, G.; Sarvazyan, N.; Sawyer, D. B. Anthracycline cardiotoxicity: from bench to bedside. *J. Clin. Oncol.* **26:**3777–3784; 2008.

[41] Hill, B. G.; Dranka, B. P.; Zou, L.; Chatham, J. C.; Darley-Usmar, V. M. Importance of the bioenergetic reserve capacity in response to cardiomyocyte stress induced by 4-hydroxynonenal. *Biochem. J.* **424:**99–107; 2009.

[42] Piscitelli, S. C.; Rodvold, K. A.; Rushing, D. A.; Tewksbury, D. A. Pharmacokinetics and pharmacodynamics of doxorubicin in patients with small cell lung cancer. *Clin. Pharmacol. Ther.* **53:**555–561; 1993.

[43] Rosenoff, S. H.; Olson, H. M.; Young, D. M.; Bostick, F.; Young, R. C. Adriamycin-induced cardiac damage in the mouse: a small-animal model of cardiotoxicity. *J. Natl. Cancer Inst.* **55:**191–194; 1975.

[44] Chaiswing, L.; Cole, M. P.; St Clair, D. K.; Ittarat, W.; Szweda, L. I.; Oberley, T. D. Oxidative damage precedes nitrative damage in adriamycin-induced cardiac mitochondrial injury. *Toxicol. Pathol.* **32:**536–547; 2004.

[45] Yen, H. C.; Oberley, T. D.; Vichitbandha, S.; Ho, Y. S.; St Clair, D. K. The protective role of manganese superoxide dismutase against adriamycin-induced acute cardiac toxicity in transgenic mice. *J. Clin. Invest.* **98:**1253–1260; 1996.

[46] David, H.; Meyer, R.; Marx, I.; Guski, H.; Wenzelides, K. Morphometric characterization of left ventricular myocardial cells of male rats during postnatal development. *J. Mol. Cell. Cardiol.* **11:**631–638; 1979.

[47] Schaper, J.; Meiser, E.; Stammler, G. Ultrastructural morphometric analysis of myocardium from dogs, rats, hamsters, mice, and from human hearts. *Circ. Res.* **56:**377–391; 1985.

[48] Hill, B. G.; Awe, S. O.; Vladykovskaya, E.; Ahmed, Y.; Liu, S. Q.; Bhatnagar, A.; Srivastava, S. Myocardial ischaemia inhibits mitochondrial metabolism of 4-hydroxy-trans-2-nonenal. *Biochem. J.* **417:**513–524; 2009.

[49] Eaton, P.; Li, J. M.; Hearse, D. J.; Shattock, M. J. Formation of 4-hydroxy-2-nonenal-modified proteins in ischemic rat heart. *Am. J. Physiol.* **276:**H935–H943; 1999.

[50] Benderdour, M.; Charron, G.; DeBlois, D.; Comte, B.; Des Rosiers, C. Cardiac mitochondrial $NADP^+$-isocitrate dehydrogenase is inactivated through 4-hydroxynonenal adduct formation: an event that precedes hypertrophy development. *J. Biol. Chem.* **278:**45154–45159; 2003.

[51] Chen, J.; Henderson, G. I.; Freeman, G. L. Role of 4-hydroxynonenal in modification of cytochrome c oxidase in ischemia/reperfused rat heart. *J. Mol. Cell. Cardiol.* **33:**1919–1927; 2001.

[52] Aitken, R. J.; Whiting, S.; De Iuliis, G. N.; McClymont, S.; Mitchell, L. A.; Baker, M. A. Electrophilic aldehydes generated by sperm metabolism activate mitochondrial reactive oxygen species generation and apoptosis by targeting succinate dehydrogenase. *J. Biol. Chem.* **287:**33048–33060; 2012.

[53] Guo, J.; Prokai-Tatrai, K.; Nguyen, V.; Rauniyar, N.; Ughy, B.; Prokai, L. Protein targets for carbonylation by 4-hydroxy-2-nonenal in rat liver mitochondria. *J. Proteomics* **74:**2370–2379; 2011.

[54] Choksi, K. B.; Nuss, J. E.; Deford, J. H.; Papaconstantinou, J. Age-related alterations in oxidatively damaged proteins of mouse skeletal muscle mitochondrial electron transport chain complexes. *Free Radic. Biol. Med.* **45:**826–838; 2008.

[55] Loeffen, J.; Elpeleg, O.; Smeitink, J.; Smeets, R.; Stockler-Ipsiroglu, S.; Mandel, H.; Sengers, R.; Trijbels, F.; van den Heuvel, L. Mutations in the complex I NDUFS2 gene of patients with cardiomyopathy and encephalomyopathy. *Ann. Neurol.* **49:**195–201; 2001.

[56] Thorn, C. F.; Oshiro, C.; Marsh, S.; Hernandez-Boussard, T.; McLeod, H.; Klein, T. E.; Altman, R. B. Doxorubicin pathways: pharmacodynamics and adverse effects. *Pharmacogenet. Genomics* **21:**440–446; 2011.

[57] Pawlowska, J.; Tarasiuk, J.; Wolf, C. R.; Paine, M. J.; Borowski, E. Differential ability of cytostatics from anthraquinone group to generate free radicals in three enzymatic systems: NADH dehydrogenase, NADPH cytochrome P450 reductase, and xanthine oxidase. *Oncol. Res.* **13:**245–252; 2003.

[58] Nicolay, K.; de Kruijff, B. Effects of adriamycin on respiratory chain activities in mitochondria from rat liver, rat heart and bovine heart: evidence for a preferential inhibition of complex III and IV. *Biochim. Biophys. Acta* **892:**320–330; 1987.

[59] Lebrecht, D.; Kokkori, A.; Ketelsen, U. P.; Setzer, B.; Walker, U. A. Tissue-specific mtDNA lesions and radical-associated mitochondrial dysfunction in human hearts exposed to doxorubicin. *J. Pathol.* **207:**436–444; 2005.

[60] Lashin, O. M.; Szweda, P. A.; Szweda, L. I.; Romani, A. M. Decreased complex II respiration and HNE-modified SDH subunit in diabetic heart. *Free Radic. Biol. Med.* **40:**886–896; 2006.

[61] Levitas, A.; Muhammad, E.; Harel, G.; Saada, A.; Caspi, V. C.; Manor, E.; Beck, J. C.; Sheffield, V.; Parvari, R. Familial neonatal isolated cardiomyopathy caused by a mutation in the flavoprotein subunit of succinate dehydrogenase. *Eur. J. Hum. Genet.* **18:**1160–1165; 2010.

[62] Olson, R. D.; Mushlin, P. S.; Brenner, D. E.; Fleischer, S.; Cusack, B. J.; Chang, B. K.; Boucek Jr. R. J. Doxorubicin cardiotoxicity may be caused by its metabolite, doxorubicinol. *Proc. Natl. Acad. Sci. USA* **85:**3585–3589; 1988.

[63] Mordente, A.; Meucci, E.; Silvestrini, A.; Martorana, G. E.; Giardina, B. New developments in anthracycline-induced cardiotoxicity. *Curr. Med. Chem.* **16:**1656–1672; 2009.

[64] Brautigam, C. A.; Chuang, J. L.; Tomchick, D. R.; Machius, M.; Chuang, D. T. Crystal structure of human dihydrolipoamide dehydrogenase: NAD^+/NADH binding and the structural basis of disease-causing mutations. *J. Mol. Biol.* **350:**543–552; 2005.

[65] Smith, D. R.; Stone, D.; Darley-Usmar, V. M. Stimulation of mitochondrial oxygen consumption in isolated cardiomyocytes after hypoxia–reoxygenation. *Free Radic. Res.* **24:**159–166; 1996.

[66] Chen, Y.; Jungsuwadee, P.; Vore, M.; Butterfield, D. A.; St Clair, D. K. Collateral damage in cancer chemotherapy: oxidative stress in nontargeted tissues. *Mol. Interv.* **7:**147–156; 2007.

[67] Kang, Y. J.; Sun, X.; Chen, Y.; Zhou, Z. Inhibition of doxorubicin chronic toxicity in catalase-overexpressing transgenic mouse hearts. *Chem. Res. Toxicol.* **15:**1–6; 2002.

[68] Zhang, S.; Liu, X.; Bawa-Khalfe, T.; Lu, L. S.; Lyu, Y. L.; Liu, L. F.; Yeh, E. T. Identification of the molecular basis of doxorubicin-induced cardiotoxicity. *Nat. Med.* **18:**1639–1642; 2012.

[69] van Dalen, E. C.; Caron, H. N.; Dickinson, H. O.; Kremer, L. C. Cardioprotective interventions for cancer patients receiving anthracyclines. *Cochrane Database Syst. Rev.* **6:**CD003917; 2011.

[70] Bloodsworth, A.; O'Donnell, V. B.; Batinic-Haberle, I.; Chumley, P. H.; Hurt, J. B.; Day, B. J.; Crow, J. P.; Freeman, B. A. Manganese–porphyrin reactions with lipids and lipoproteins. *Free Radic. Biol. Med.* **28:**1017–1029; 2000.